ICAS-88-6.3.2

THICKNESS EFFECTS IN THE UNSTEADY AERODYNAMICS OF INTERFERING LIFTING SURFACES

L. P. Ruiz-Calavera
Research Engineer
INTA
Departamento de Aerodinámica
28850 Torrejón de Ardoz
(Madrid), SPAIN

Dr. W. Geissler
Head of Unsteady Aerodynamics Branch
DFVLR
Institut für Aeroelastik
Bunsenstrasse 10
3400 Göttingen, FRG

Abstract

A panel method, originally developed to calculate steady and unsteady pressure distributions on harmonically oscillating wings in incompressible flow, has been generalized to study interference configurations. Differing from normaly used mean-surface theories, in this method the geometric boundary condition is matched on the real body surface, thus taking into account thickness effects. Application is made to three different cases: T-Tail, Wing-Tail and Engine-Wing interference. The influence of thickness is discussed comparing the results of the present method with other linearized methods as well as with experimental data.

Nomenclature

x,y,z	Cartesian Coordinates
b	Span
c	Local chord
l	Reference length
s	Coordinate along wake
S	Surface
$\vec{n}$	Unit vector normal to surfaces
t^*	Dimensionless time $t^*=tU_\infty/l$
U_∞	Reference velocity
$\vec{V}_{kin}$	Kinematic velocity
C_p	Pressure coefficient
C_y	Lateral force coefficient
C_z	Vertical force coefficient
C_{mx}	Rolling moment coefficient

Greek Symbols

ω^*	Reduced frequency $\omega^*=\omega\, l/U_\infty$
ϕ	Perturbation potential
$\bar{\alpha}$	Mean angle of attack
α'	Amplitude of oscillation (Pitch)
$\bar{\psi}$	Mean Yaw angle
ψ'	Amplitude of oscillation (Yaw)
Δ	Difference

Sub- and Superscripts

$(\ )_f$	Fin
$(\ )_s$	Stabilizer
$(\ )_w$	Wing or wake
$(\ )_t$	Tail
$(\ )_e$	Engine
$(\_)_{te}$	Trailing Edge
$(\bar{\ })$	Mean or steady part
$(\ )'$	Real part
$(\ )''$	Imaginary part

I. Introduction

It is well established both by theory and experiment that the unsteady aerodynamic forces needed for flutter analysis are markedly influenced by the mutual interference between lifting surfaces. This phenomenon occurs not only when these interacting surfaces are close together, but also when one of them is located near the wake of the other.

A velocity potential panel method, originally developed to calculate steady and unsteady pressure distributions on harmonically oscillating isolated wings in incompressible flow [1], has been further extended to take into account more than one lifting surface, thus allowing to study interference problems. Differing from the normaly used mean-surface theories [2] in this method the kinematic boundary condition is imposed on the real wings surfaces. Furthermore, no linearization is applied to this condition or to Bernoulli's equation. In this way the method effectively allows to evaluate non-linear influences such as thickness and steady solution effects, on the unsteady loads of interference configurations.

Calculations are presented for three different cases, namely: T-Tail, Wing-Tail and Engine-Wing interference, each of which introduces a different mechanism for the influence of thickness. The results of the method are compared with other methods as well as with experimental data when available.

II. Method Description

In ([1]) a velocity potential panel method to calculate unsteady pressure distributions around isolated thick wings oscillating in incompressible flow was presented. A short description follows. Under the assumption of harmonic oscillations of small amplitude, and retaining first order terms in the amplitude only, the kinematic boundary condition at the surface of a translating and oscillating wing can be separated into a mean or steady part and a first harmonic or unsteady part for which the usual complex notation is used.

$$\vec{V}_{kin} = \bar{\vec{V}}_{kin} + (\vec{V}'_{kin} + i\,\vec{V}''_{kin})\, e^{i\omega^* t^*} \qquad (1)$$

Correspondingly, the problem -which satisfies Laplace's equation- can be expressed in terms of steady and unsteady perturbation potentials by superposition.

$$\phi = \bar{\phi} + (\phi' + i\,\phi'')\, e^{i\omega^* t^*} \qquad (2)$$

These potentials must fulfill the exact kinematic boundary condition on the real surface of the wings

$$\frac{\partial \bar{\phi}}{\partial n} = \bar{\vec{V}}_{kin} \cdot \vec{n} \qquad (3)$$

$$\frac{\partial(\phi' + i\,\phi'')}{\partial n} = (\vec{V}'_{kin} + i\,\vec{V}''_{kin}) \cdot \vec{n}$$

and the additional conditions that the wakes behind the wings -which are assumed to be flat and in the direction of half the mean angle of attack- cannot sustain any pressure difference across them, and that a Kutta Condition (no pressure jump) must be satisfied at the trailing edges.

The steady and unsteady problems are coupled via the kinematic boundary condition and Bernoulli's equation, in such a way that the steady part influences the unsteady but not vice versa (due to the assumption of small amplitude of oscillation).

The problem is solved using a first order panel method. The surfaces of the wings are represented by a large number of small quadrilateral panels (Fig.1 shows one of the lifting surfaces) which are arranged in streamwise sections. These sections are extended into the wakes; thus forming semi-infinite wake strips. Each panel on the wing is covered with constant source and doublet distribu- tions of both steady and pulsating type. Whereas the source panels have independent strengths, the doublet panel strenghts are related in such a way that only a free parameter per strip remains, namely the circulation around that section. The wake strips are covered with both steady and pulsating doublets whose spatial distribution of intensity can be related to the temporal history of the circulation around the corresponding section by means of the dynamic condition of the wakes (no pressure jump across them).

$$\Delta\bar{\phi}_w = \Delta\bar{\phi}_{te} \qquad (4)$$

$$\Delta(\phi' + i\,\phi'')_w = \Delta(\phi' + i\,\phi'')_{te}\, e^{i\omega^*(s-s_{te})}$$

The steady and pulsating source intensities are obtained fulfilling the kinematic boundary conditions (3) in a control point per panel. In this way two systems of linear equations are produced. The steady and unsteady circulations around the different wing sections, and with it the strength of the steady and pulsating doublets on the wake strips, are determined by application of the Kutta condition at each strip. The condition of no pressure jump at the trailing edge is fulfilled for both the steady and the unsteady parts separately. In the steady case, this condition leads to a quadratic system of equations (which is solved numerically) and in the unsteady case to a linear system of equations.

Once the strengths of the different sigularities have been obtained, the potential and velocities at any point can be calculated, and the pressures can be determined by means of Bernoulli's equation (posed in a body fixed reference system)

$$C_p = -\frac{2}{U_\infty^2}\left(\frac{\partial \phi}{\partial t} + \frac{1}{2}\left|\nabla\phi\right|^2 - \nabla\phi \cdot \vec{V}_{kin}\right) \qquad (5)$$

which can also be separated into steady and unsteady parts

$$C_p = \bar{C}_p + (C'_p + i\,C''_p)\, e^{i\,\omega^* t^*} \qquad (6)$$

The method has been further generalized to take into account more than one lifting surface, thus allowing to study interference effects. The wake strip unsteady influence functions -which constitute the most difficult part of the calculation and have to be numerically evaluated- have been modified to improve its accuracy when applied to the very different configurations possible in interference problems. Furthermore an analytical solution of the unsteady wake influence integral ([3]) which is valid for wings without trailing edge sweep, was adapted and included in the method. This brings considerable savings

in computing time.

Two different procedures are used to solve the interference problems. When the various lifting surfaces are closely coupled (e.g. T-Tails) a direct approach is selected, that is, all the lifting surfaces are solved at the same time, with the corresponding cost in computing time and memory. On the other hand, whenever the interference among the lifting surfaces is not direct (e.g. in a wing-tail interference case for which the interaction is mainly via the wing wake) an iterative procedure between the different lifting surfaces is employed, which saves a lot of computer resources.

III. T-Tail

The method has been first applied to a simplified T-Tail configuration with square surfaces which is oscillating in yaw about an axis through the midchord of the vertical fin (Fig.2). For this tail, measured data already exist (4) and comparative calculations have been carried out by other authors (5,6).

The surfaces were modeled using a total of 960 panels distributed in 10 sections of 40 panels around a NACA 65A010 profile on the fin and 12 sections of 40 panels around a NACA 65A010 profile on the stabilizer. Since there was no flow around the side edge of the fin during the measurements, the image principle was employed for the calculation, the fin being reflected on its base. Only 2 strips of 40 panels were used on this surface. As the mean yaw angle was zero only the right half of the configuration had to be considered by imposing anti-symmetry conditions at the vertical plane.

Fig.3 shows the pressure distribution (mean, real and imaginary parts) around a fin section at 80% span for a reduced frequency (based on the semi-chord) of 0.5. Also represented are the results obtained with a previously developed (7) fully linearized version of the velocity potential panel method, based on a theory described in (8). In this case the wings are represented by their infinitely thin mean surface, on which the kinematic boundary condition is applied. These mean surfaces are modeled using constant strength doublet panels. This linearization leads to a complete separation of the problem into a steady and an unsteady part. The differences between both methods are therefore due to the thickness effect and in a lesser extend to the non linearity of Bernoulli's equation and the coupling of steady and unsteady solutions (these effects would have been larger had the tail had a mean yaw angle).

Due to the anti-simmetry only the pressures on one side of the fin are shown. The qualitative behaviour of the discrepancies between both methods is very similar to that found in wing alone cases (1). In the front part of the section the real parts of the pressures predicted by the linearized method are lower and have a steep gradient at the leading edge due to the square root singularity there. At the aft position, the linearized pressures are slightly larger in comparison with the nonlinearized values. For the imaginary part, the larger differences appear in the neighbourhood of the trailing edge. These discrepancies are due to the direct effect of thickness on the corresponding oscillating lifting surface.

Fig.4 shows the pressure distribution along the chord of a stabilizer section at 60% semi-span. In order to compare results with the linearized method the pressure difference (lifting pressure) is represented. Once again the discrepancies are readily apparent. In this case a new effect is involved, namely the kinematic velocities at the stabilizer leading edge due to its thickness and the yawing motion, which are not taken into account by the mean-surface theories.

The differences in the pressures reflect in the lift distributions along the span of both fin and stabilizer as shown in Fig.5. In Figs.6 and 7 amplitude and phase angles of the global forces predicted by the present method are plotted versus reduced frequency and compared with measured data (4) and results obtained by other mean-surface theories (5,6). The lateral force is studied in Fig.6. It can be seen that although the amplitude of the force is not very much affected, the phase angle is considerably diminished, which reduces the discrepancies with the experimental data. The still remaining differences can be attributed (9) to incomplete representation of the tunnel walls and viscous effects (it is thought that the inclusion of the boundary layer displacement thickness in a similar way to that used in (1) would further approximate the theoretical results to the experimental ones). Similar conclusions can be reached for the stabilizer rolling moment (Fig.7).

IV. Wing-Tail Interference

Next a wing-tail interference case is studied. The configuration selected Fig.8 is that measured in (10). The model consisted of a semi-wing and co-planar tail unit fixed to a tunnel wall. The wing could be swept into three different positions. Only results for the 25º sweep position are shown. The wing had a NACA 64A012Q13 profile. Due to the author's lack of information on this profile a NACA 64A012 section was instead used for the calculations. Furthermore the assumption was made that this section was parallel to the incoming flow for the wing with 25º sweep. This point could not be confirmed and no information could be found in the

original report. The tail had a NACA 64A0041/2 profile. The wing oscillates in pitch about its 40% axis with a reduced frequency (based on the wing center-chord) of 1.212. Mean angle of attack was zero. The tail does not oscillate so that all the unsteady loads on it are induced by the wing wake. The influence of the tail on the wing is very small. The semi-wing was modeled using 500 panels arranged in 10 strips of 50 panels around the NACA 64A012 profile. The tail is so thin (4'5%) that it was modeled using a mean-surface representation without thickness. Symmetry conditions were imposed at mid-plane to represent the tunnel wall.

Fig.9 shows the chordwise lifting pressure distribution on a tail section at 70% semi-span calculated by the present method and by the linearized version. Once again differences appear, specially in the imaginary part. As in both calculations the tail model is exactly the same the reason for the discrepancies must be sought in the forcing mechanism, that is, the wing wake. In Fig.10 the potential difference between the upper and lower sides of the wing at the same spanwise station (wing section 30'43%) is presented. Whereas the real parts compare very well with the linearized results, this is not the case for the imaginary parts. Specially important is the potential jump at the trailing edge, that is, the circulation around that section, which controls the wake strength. Fig.11 shows the spanwise distribution of this variable. It can be seen that thickness effects produce a phase lag when compared with linearized results. The amplitude is almost not affected. A phase lag in the wake strength is effectively equivalent to a change in the separation between wing and tail, and the pressures on the tail are very sensible to tail position ([10]). Summarizing, the discrepancies in the loads on the tail -which reduce to a phase lag- can be attributed to the influence of wing thickness effect on the wake strength.

As for the comparison with experimental results, it can be seen (Fig.9) that a much better agreement is reached for the imaginary part, whereas no net improvement in the real part is appreciated by the inclusion of thickness effects. That is, a change in the phase of the wake strength produces a change in the phase of the loads on the tail without affecting its amplitude too much.

V. Engine-Wing Interference

The present method has been coupled with an engine model ([11]) in order to study an engine-wing interference case. Conical panels are used to represent the engine, which has no thickness. The jet effect is also included by means of a vortex tube.

Fig.12 shows a simplified theoretical configuration selected as a test case. No experimental data are available. The engine oscillates in pitch about its center point with a reduced frequency (based on engine length) of 1.0. The wing, with a NACA 0012 profile, has no oscillation of its own so that all the unsteady forces on it are induced by the engine wake and jet. The pressure distribution on the wing has been calculated using the present method and the linearized version. In both cases the same engine model is used and furthermore, no influence of the wing on the engine is considered. In this way it is possible to evaluate the influence of thickness on the loads induced by a definite unsteady flow field.

Three different cases are considered. In the first one (Fig.13) the engine has neither mean angle of attack nor jet. In the second (Fig. 14) the engine has a mean angle of attack of 5º and no jet. Finally in the third case (Fig.15) the engine has no mean angle of attack but has a jet velocity of five times the incident velocity. In the three cases the engine oscillation is exactly the same.

Figures 13 to 15 show the distribution of lifting pressures (mean part and first harmonic) along the wing mid-chord, calculated by both methods. The discrepancies arise from the fact that the velocities induced by the wake and jet will be imposed as kinematic boundary condition on different points and with different normal unit vectors. Noteworthy are the large changes in both the steady and unsteady solutions associated with the presence of the jet. This point deserves further investigation.

VI. Conclusions

The effect of thickness on the unsteady aerodynamics of interfering lifting surfaces has been studied. Three configurations have been considered and different mechanisms for thickness influence have been identified: Thickness direct influence on an oscillating lifting surface, thickness influence on the strength of a wake which induces unsteady loads, and thickness influence on the loads induced by a definite unsteady flow field. It appears that the main effect of thickness is on the phase lag of the loads. Amplitude of the loads does not seem to be so much affected. This explains some of the differences found in comparisons between experimental data and the results of linearized methods.

References

(1) Geissler, W. "Nonlinear Unsteady Potential Flow Calculations for Three Dimensional Oscillating Wings". AIAA Journal, Vol. 16, No.11, Nov.1978 pp.1168-1174.

(2) Rodden, W.P. "A Comparison of Methods used in Interfering Lifting Surface Theory" AGARD-R-643, 1976.

(3) Send, W. "Der instationäre Nachlauf hinter Schlanken Auftriebskörpern in inkompressibler Strömung" ZAMM 64.7-15 (1984).

(4) Clevenson, S.A. Leadbetter, S.A. "Measurements of Aerodynamic Forces and Moments at Subsonic Speeds on a Simplified T-Tail Oscillating in Yaw about the Fin Midchord" NACA TN 4402, Sept.1958

(5) Rodden, W.P. Albano, E. "The Subsonic Aerodynamic Loads on a Simplified T-Tail Oscillating in Yaw -Summary of Calculations and Comparisons with Experiment" NOR 68-126 (1968)

(6) Böhm, G. Schmid, H. "Subsonic Unsteady Airloads on Multiple Lifting Surfaces" AGARD CP-80-71 (1970).

(7) Ruiz-Calavera, L.P. "A Velocity Potential Panel Method for Harmonically Oscillating Interfering Lifting Surfaces" V International Conference on Numerical Methods in Laminar and Turbulent Flows. Montreal, Canada, 6th-10th July 1987.

(8) Jones, W.P. Moore, J.A. "Simplified Aerodynamic Theory of Oscillating Thin Surfaces in Subsonic Flow" AIAA Journal Vol.11, No.9, Sept.1973, pp.1305-1309.

(9) Zwaan, R.J. "Calculated Results for Oscillating T-Tails in Subsonic Flow and Comparison with Experiments". NLR-Rep. MP.253 (1967).

(10) Triebstein, H. Wagener, J. "Druckverteilungsmessungen an harmonisch schwingenden Flügel-Höhenleitwerks Kombinationen". DFVLR 71 J 02 (1971).

(11) Katzer, E "Steady and Unsteady Potential Flows around axisymmetric bodies and ring airfoils". 3rd GAMM-Seminar. "Panel Methods in Mechanics". Kiel. 16-18, January, 1987.

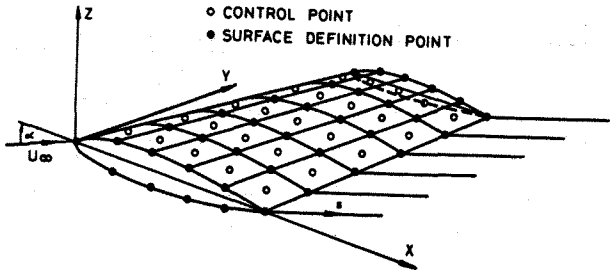

Fig.1 Wing Surface Discretitation

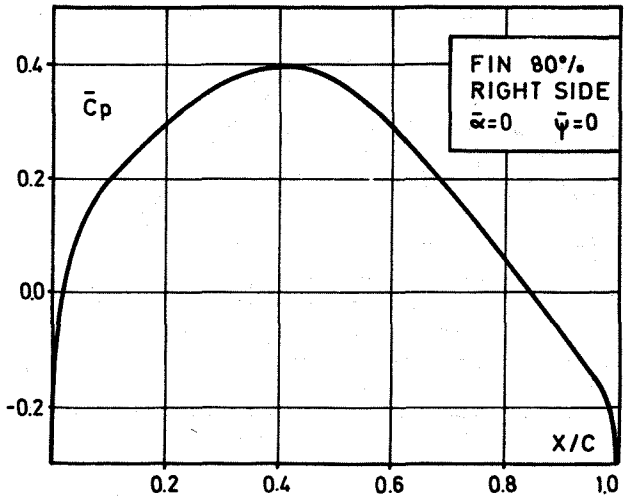

Mean Part of Pressure Coefficient

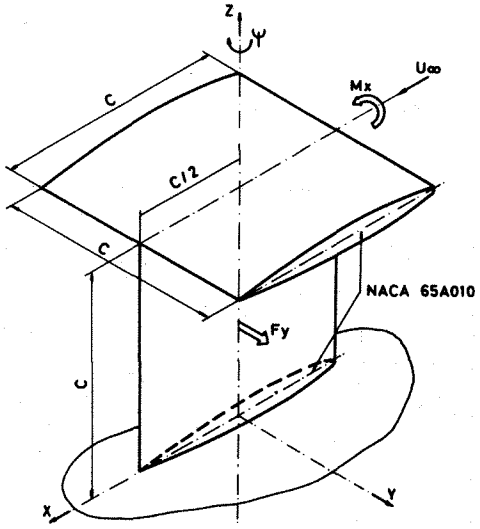

Fig. 2 NACA TN 4402 YAWING T-TAIL CONFIGURATION INDICATING SIGN CONVENTION

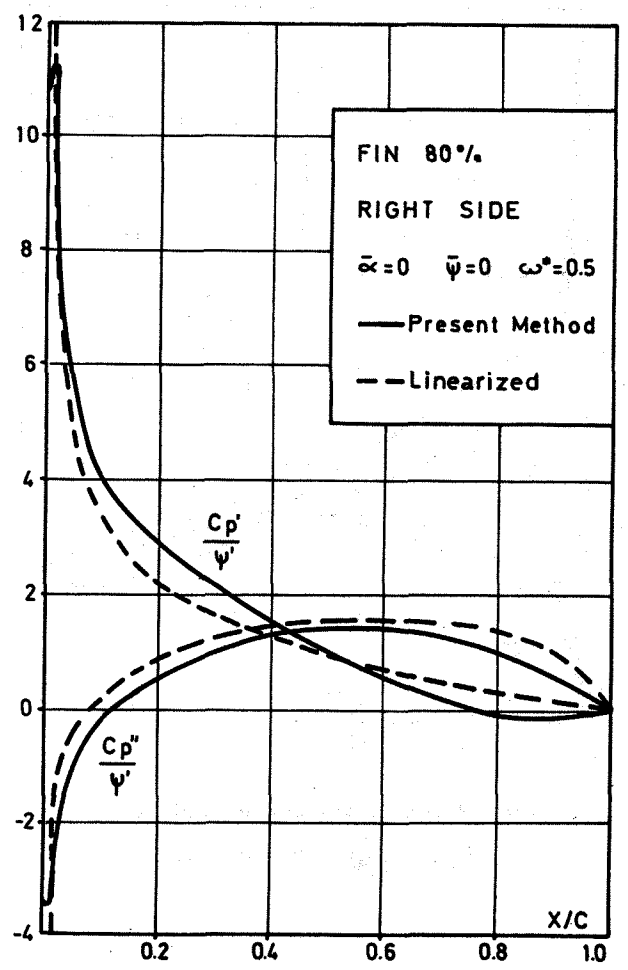

First Harmonic of Pressure Coefficient

Fig.3 T-TAIL INTERFERENCE

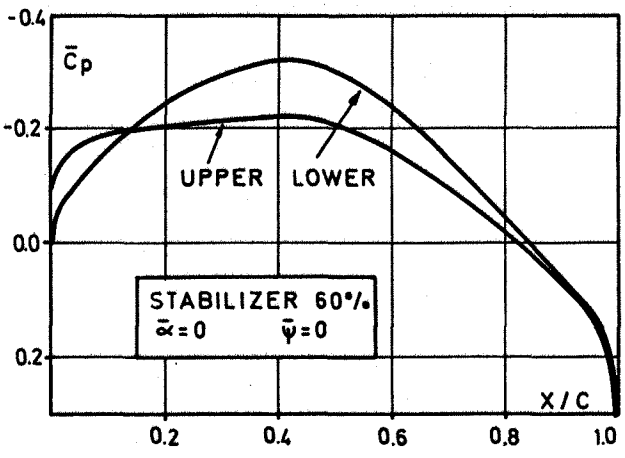

Mean Part of Pressure Coefficient

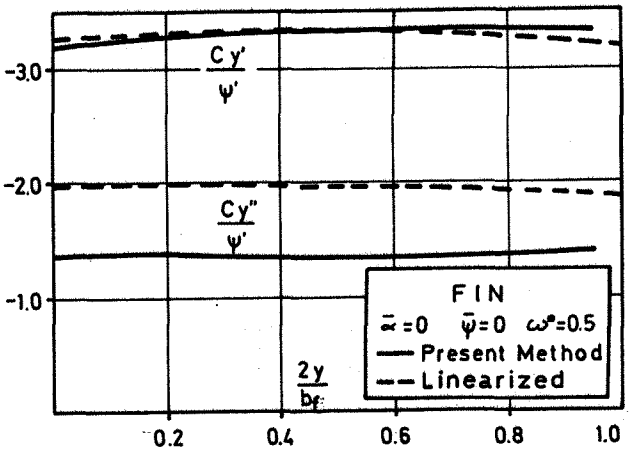

Fin Side Force Coefficient

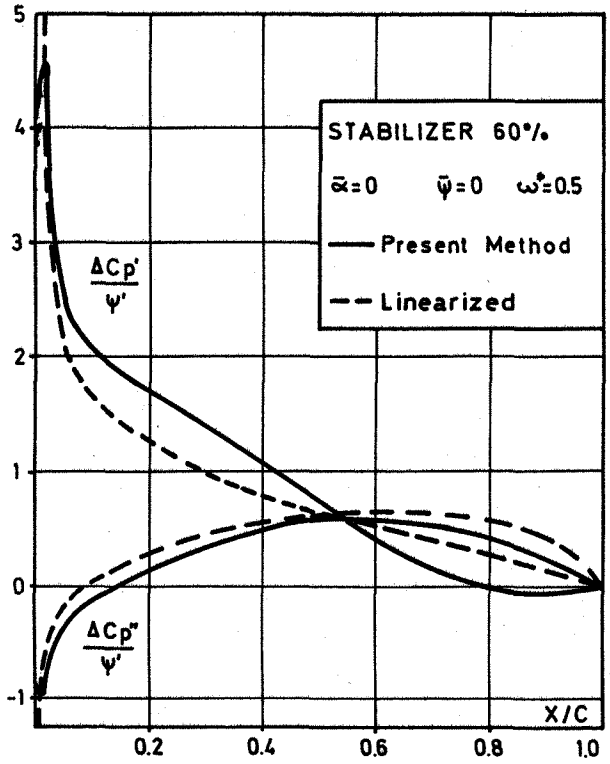

First Harmonic of Pressure Coefficient

Fig.4 T-TAIL INTERFERENCE

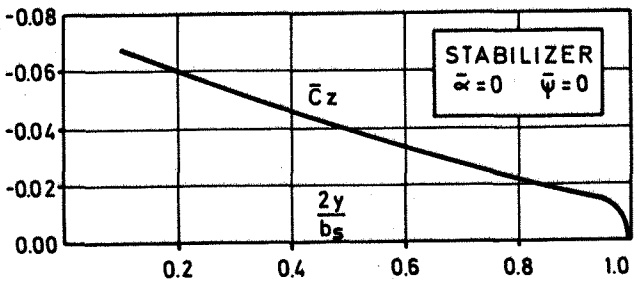

Stabilizer Lift Coefficient. Mean Part

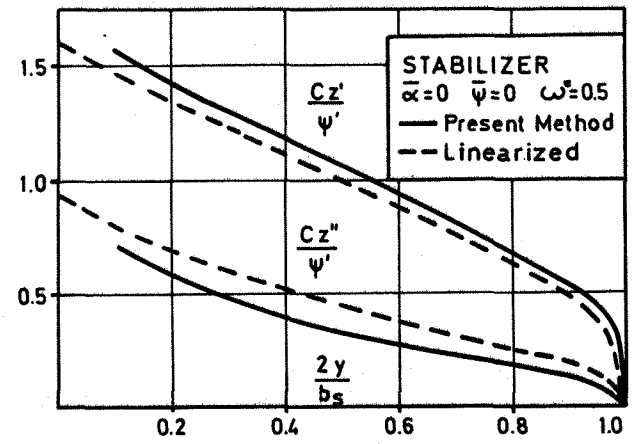

Stabilizer Lift Coefficient. First Harmonic

Fig. 5 T-TAIL INTERFERENCE

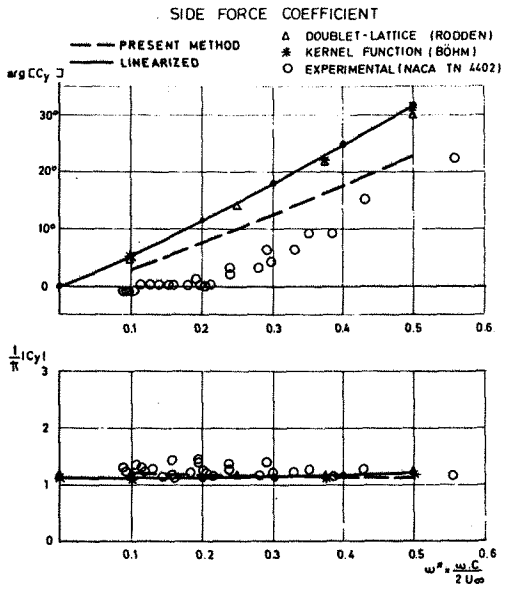

Fig.6 T-TAIL INTERFERENCE

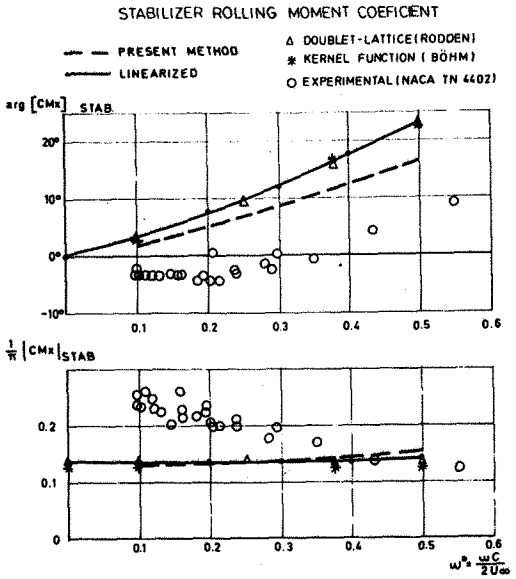

Fig. 7 T-TAIL INTERFERENCE

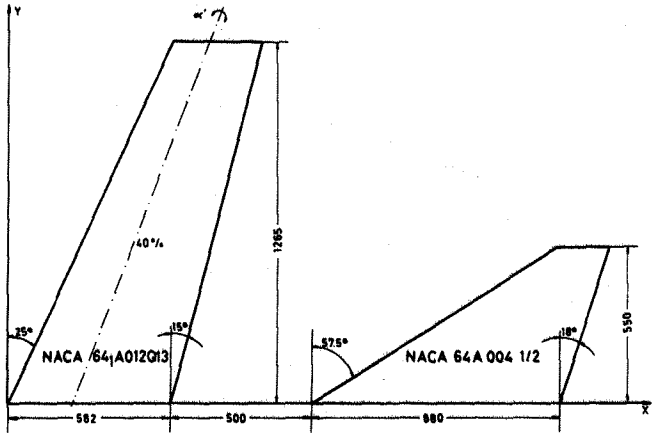

Fig. 8 WING-TAIL CONFIGURATION

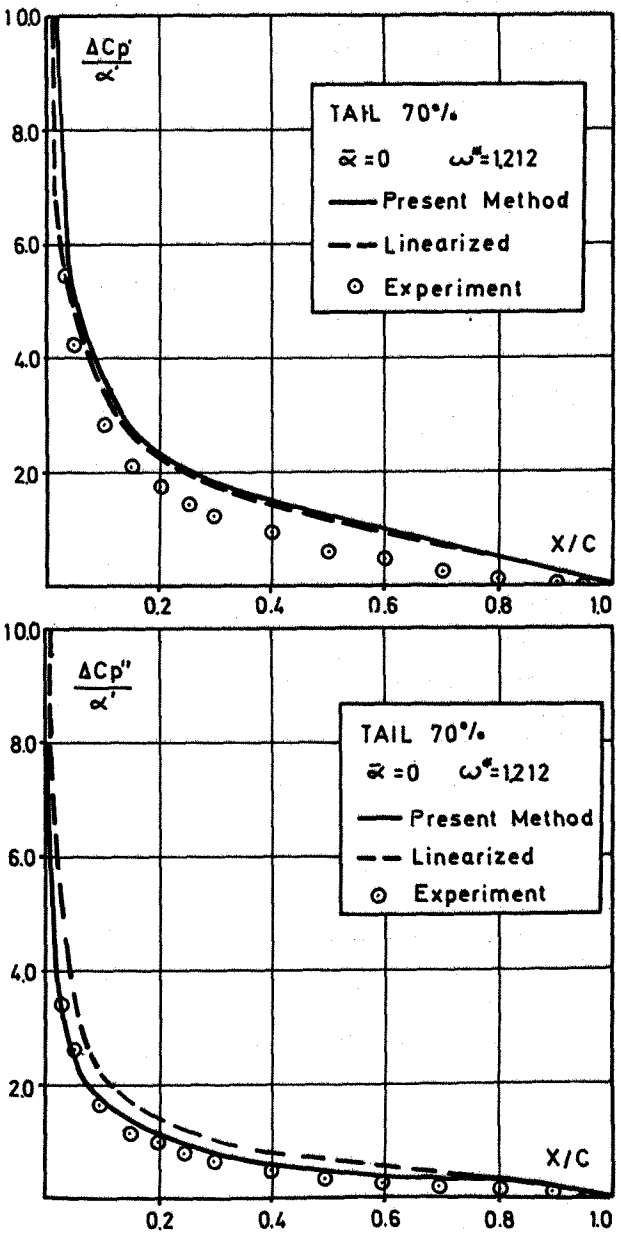

Fig.9 WING-TAIL INTERFERENCE

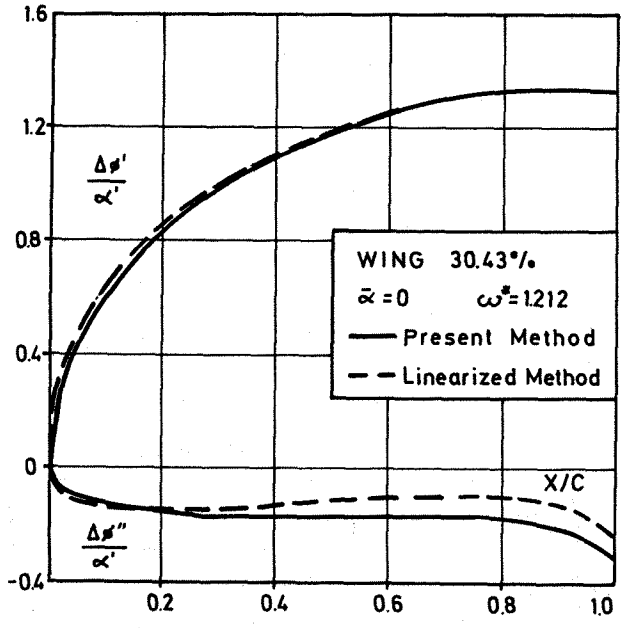

Fig.10 WING-TAIL INTERFERENCE

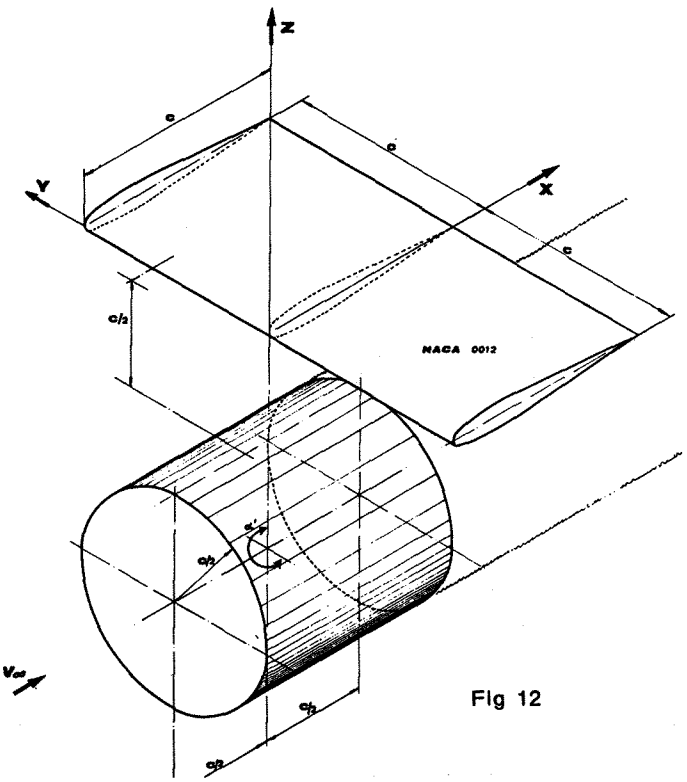

Fig 12

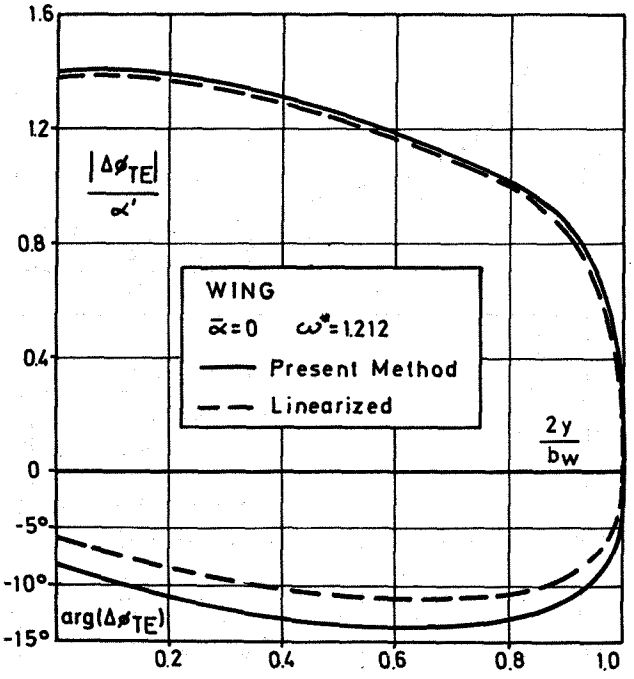

Fig. 11 WING-TAIL INTERFERENCE

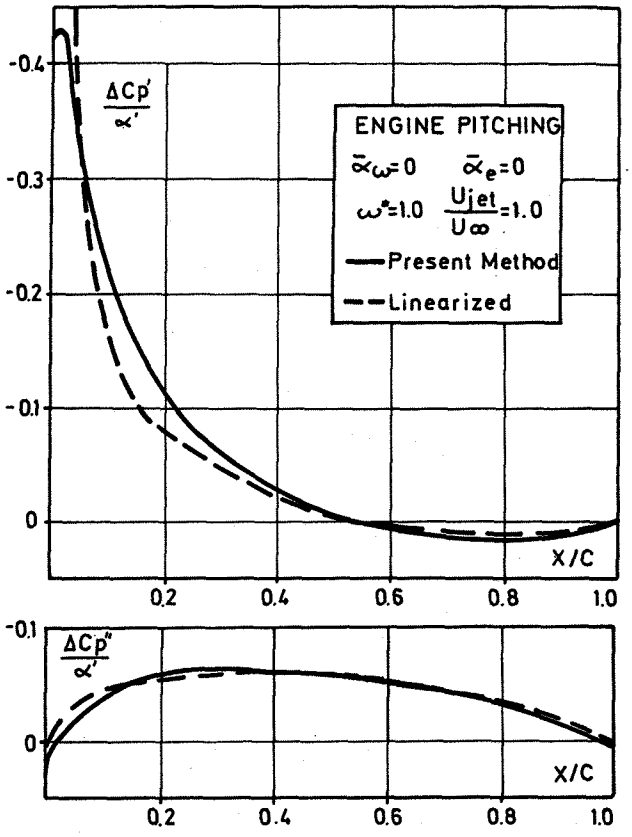

Fig.13 ENGINE-WING INTERFERENCE

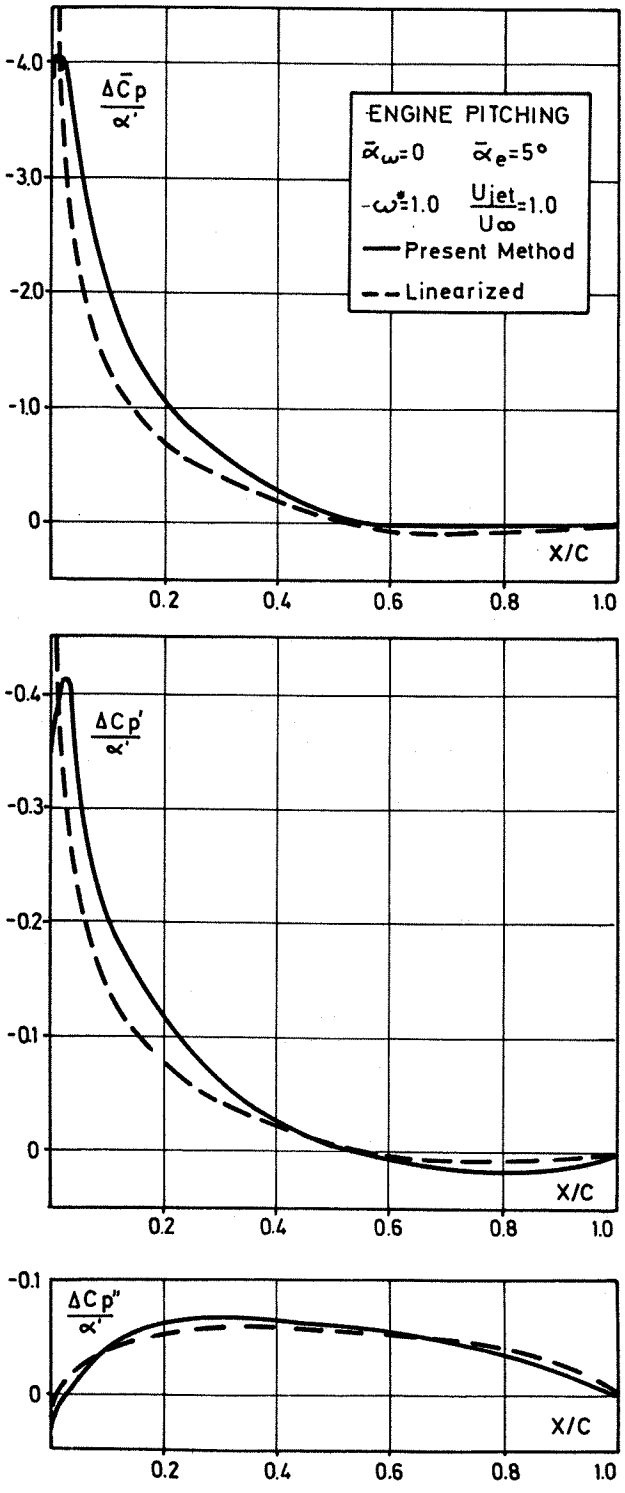

Fig. 14 ENGINE-WING INTERFERENCE

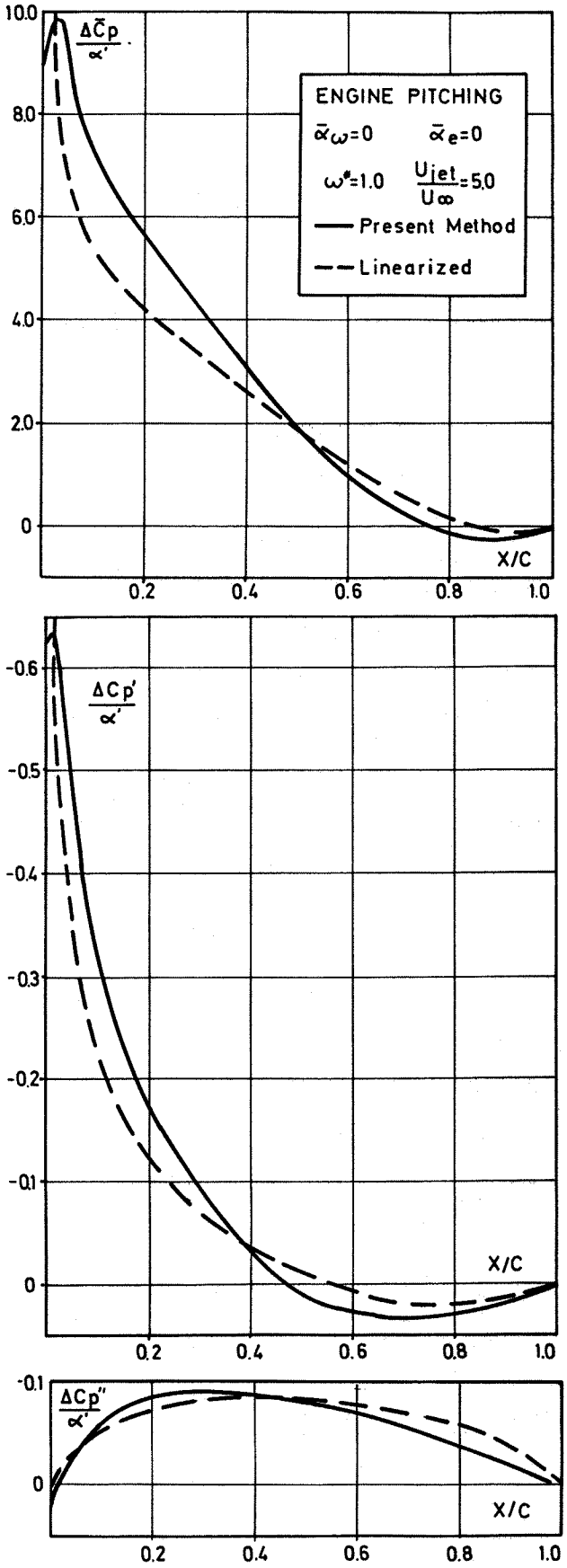

Fig.15 ENGINE-WING INTERFERENCE